The missing dwarf galaxies of the Local Group

Azadeh Fattahi [ID],[1][*] Julio F. Navarro[2][†] and Carlos S. Frenk[1]

[1]*Department of Physics, Institute for Computational Cosmology, University of Durham, South Road, Durham DH1 3LE, UK*
[2]*Department of Physics and Astronomy, University of Victoria, PO Box 3055 STN CSC, Victoria, BC V8W 3P6, Canada*

ABSTRACT

We study the Local Group (LG) dwarf galaxy population predicted by the APOSTLE ΛCDM cosmological hydrodynamics simulations. These indicate that: (i) the total mass within 3 Mpc of the Milky Way–Andromeda mid-point ($M_{3\mathrm{Mpc}}$) typically exceeds $\sim$3 times the sum of the virial masses ($M_{200\mathrm{crit}}$) of the two primaries and (ii) the dwarf galaxy formation efficiency per unit mass is uniform throughout the volume. This suggests that the satellite population within the virial radii of the Milky Way and Andromeda should make up fewer than one third of all LG dwarfs within 3 Mpc. This is consistent with the fraction of observed LG galaxies with stellar mass $M_* > 10^7\,\mathrm{M_\odot}$ that are satellites (12 out of 42; i.e. 28 per cent). For the APOSTLE galaxy mass–halo mass relation, the total number of such galaxies further suggests an LG mass of $M_{3\mathrm{Mpc}} \sim 10^{13}\,\mathrm{M_\odot}$. At lower galaxy masses, however, the observed satellite fraction is substantially higher (42 per cent for $M_* > 10^5\,\mathrm{M_\odot}$). If this is due to incompleteness in the field sample, then $\sim$50 dwarf galaxies at least as massive as the Draco dwarf spheroidal must be missing from the current LG *field* dwarf inventory. The incompleteness interpretation is supported by the pronounced flattening of the LG luminosity function below $M_* \sim 10^7\,\mathrm{M_\odot}$, and by the scarcity of low surface brightness LG field galaxies compared to satellites. The simulations indicate that most missing dwarfs should lie near the virial boundaries of the two LG primaries, and predict a trove of nearby dwarfs that await discovery by upcoming wide-field imaging surveys.

Key words: galaxies: abundances – galaxies: dwarf – Local Group – galaxies: luminosity function, mass function – dark matter.

1 INTRODUCTION

The inventory of galaxies in the surroundings of the Milky Way (MW) and Andromeda (M31) galaxies is almost certainly incomplete. Every new wide-field imaging survey of the night sky, when combined with refined galaxy finding techniques, yields almost inevitably a plentiful catch of new discoveries, many of which have been MW and M31 satellites (see e.g. Belokurov et al. 2007, 2010; McConnachie et al. 2008; Bechtol et al. 2015; Drlica-Wagner et al. 2015; Koposov et al. 2015). In the case of the MW, for example, satellites as faint as $M_V \sim -2$ have now been reported, extending by several orders of magnitude the faint-end limit of the galaxy luminosity function to a 'confusion-limited' regime where faint galaxies and star clusters become indistinguishable from each other without accurate kinematic data (Simon & Geha 2007; Tolstoy, Hill & Tosi 2009; Koposov et al. 2011; McConnachie 2012; Martin et al. 2016; Walker et al. 2016; Simon 2019).

These newly discovered satellites are not just faint but have also extremely low surface brightness (LSB), reaching values $\sim$100 times fainter than the 'ultradiffuse' galaxy population (UDG) recently reported in galaxy clusters and in the vicinity of bright galaxies (van Dokkum et al. 2015; Yagi et al. 2016). These extreme LSB dwarfs are rather challenging to detect and, consequently, the census of faint satellites around the MW and M31 is widely agreed to be far from complete (Newton et al. 2018; Nadler et al. 2019). Correcting for this incompleteness is non-trivial, for it requires making assumptions about how satellites populate the size–luminosity plane, as well as how they are distributed radially, neither of which is known accurately enough (Koposov et al. 2008).

The incompleteness is often thought to affect solely the 'ultrafaint' regime, defined here as galaxies below $M_V \sim -8$ (or a stellar mass of $M_* \sim 10^5\,\mathrm{M_\odot}$; i.e. that of the Draco, or Ursa Minor, dwarf spheroidals; hereafter dSphs). However, the recent discovery of 'feeble giant' galaxies, such as the Crater II and Antlia II dSphs (Torrealba et al. 2016, 2018), suggests that our current inventory of MW satellites may be missing systems even in the $M_V < -8$ luminosity range typically referred to as 'classical dSphs'.

[*] E-mail: azadeh.fattahi-savadjani@durham.ac.uk
[†] CIfAR Fellow.

Galaxies like Crater II have unexpectedly large radii, making them practically invisible through the foreground of Galactic stars and the background of distant galaxies.

Although difficult to detect, these ultradiffuse systems have the potential of yielding important clues to our understanding of dwarf galaxy formation. Indeed, the kinematics of their stars have proved challenging to interpret: some have extremely low velocity dispersions, hinting at very low dark matter densities (e.g. Crater II, And XIX, Collins et al. 2013; Caldwell et al. 2017), while others inhabit surprisingly dense haloes, according to the kinematical evidence (e.g. Draco, Tucana, Walker et al. 2007; Gregory et al. 2019). These diverse properties are mirrored by other UDGs outside the Local Group (LG), where some have been associated with massive dark haloes (Beasley et al. 2016; van Dokkum et al. 2016), whereas others have been found to contain little obvious evidence for dark matter (van Dokkum et al. 2018).

It would be extremely valuable to find other examples of such systems in the LG, as their proximity facilitates their study. Particularly interesting are luminous dwarfs such as the 'feeble giants' mentioned above, where the large number of giant stars amenable to spectroscopic observation would enable detailed modelling that may shed light on the origin of their puzzling kinematics.

We address these issues here using cosmological hydrodynamical simulations of LG-like volumes from the APOSTLE[1] project (Fattahi et al. 2016; Sawala et al. 2016b). In particular, we aim to estimate the number of 'classical dSphs' (i.e. those with $M_V < -8$, or, equivalently, $M_* > 10^5 \, \mathrm{M_\odot}$) in the LG volume, defined here as the 3 Mpc-radius sphere around the mid-point between the MW and M31. As we discuss below, this depends primarily on the total mass within that volume, and on whether the dwarf galaxy formation 'efficiency' (i.e. the number of galaxies per unit mass) in that volume is substantially different from that of the MW halo.

The plan for this paper is as follows. After describing the simulations (Section 2) and galaxy samples (Section 3) we consider in our study, we analyse the galaxy formation efficiency in the LG field and around the two primaries (Section 4). The analysis contrasts the expected faint end of the LG luminosity/stellar mass function with current observational constraints, and yields an estimate of the total mass within 3 Mpc (Section 4.5); a prediction for the number of luminous dwarfs missing from that volume (Section 4.6); and clear indications as to where they might be located (Section 4.7). We end with a brief discussion of the surface brightness limits of current samples of satellites and field LG galaxies, which clearly demonstrates the lack of known LSB galaxies in the LG field.

2 NUMERICAL SIMULATIONS

2.1 The DOVE simulation

We use the DOVE *N*-body cosmological simulations (Jenkins 2013), to select LG-like environments. DOVE followed evolution of a $100^3 \, \mathrm{Mpc^3}$ cosmological cube with 1620^3 collisionless dark matter particles of mass $m_p = 8.8 \times 10^6 \, \mathrm{M_\odot}$. The simulation started at redshift $z = 127$ and was run to $z = 0$ with the Tree-PM code P-GADGET3, a variant of the publicly available code, GADGET-2 (Springel et al. 2005). DOVE adopts flat lambda cold dark matter (ΛCDM) cosmological parameters consistent with WMAP-7 data (Komatsu et al. 2011): $h = 0.704$, $\Omega_m = 0.272$, $\Omega_{bar} = 0.045$.

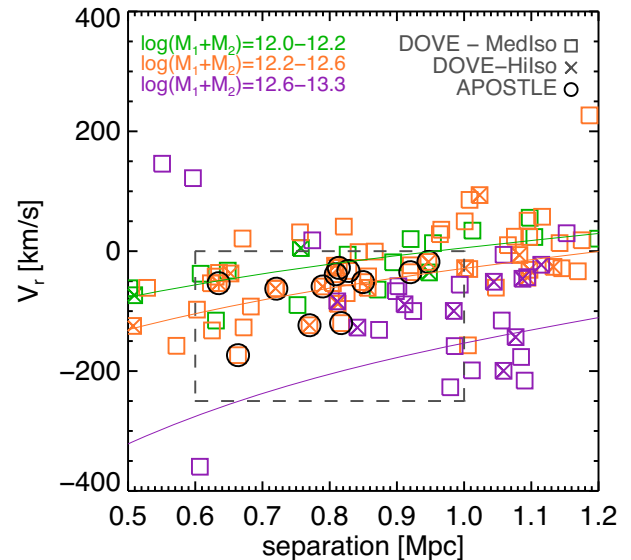[1] A Project Of Simulating The Local Environment

Figure 1. Relative radial velocity versus separation of halo pairs in the DOVE cosmological simulation. Squares and crosses correspond to the medium-isolation (MedIso) and high-isolation (HiIso) criteria. APOSTLE candidates are highlighted with circles. Solid curves indicate the timing argument solutions of $\log(M_1 + M_2)/\mathrm{M_\odot} = 12.1$, 12.4, and 13 coloured in green, orange, and purple, respectively. Similarly, DOVE pairs are colour coded in the same way, according to the combined virial mass of the pair, $M_1 + M_2$. The box shows the radial velocity and separation criteria chosen to select LG-like pairs.

DM haloes are identified in DOVE at $z = 0$ using the friends-of-friends algorithm (FoF; Davis et al. 1985) with linking length 0.2 times the mean interparticle separation. Bound structures and substructures in FoF haloes are found recursively using SUBFIND (Springel, Yoshida & White 2001).

We search for LG-like environments in DOVE by considering all haloes with virial[2] mass above $5 \times 10^{11} \, \mathrm{M_\odot}$ and identifying pairs with separations $\sim 800 \, \mathrm{kpc}$. The pair members are typically in separate FoF groups but in some cases they are linked into a single FoF halo.

We select pairs that meet a relatively strict isolation criterion ('MedIso') so that there are no haloes more massive than the lower mass pair member within $d_{iso} = 2.5 \, \mathrm{Mpc}$ from the mid-point between the primaries.[3] A more restrictive isolation criterion ('HiIso') was also considered, with $d_{iso} = 5 \, \mathrm{Mpc}$.

Fig. 1 shows the separation and relative radial velocity (V_r) of DOVE pairs. Systems identified with the 'MedIso' and 'HiIso' isolation criteria are represented with open squares and crosses, respectively. (HiIso pairs are a subsample of the MedIso sample, by definition). The pairs are colour coded according to the sum of the virial mass of the paired haloes, $M_1 + M_2$. The solid curves indicate the expected loci of pairs of fixed total mass on radial orbits, according to the timing argument (Kahn & Woltjer 1959; Li & White 2008; Fattahi et al. 2016).

We narrow down the pair selection by applying constraints on separation, $600 < r / \mathrm{kpc} < 1000$, and radial velocity, $-250 <$

[2] We define the virial boundary of a halo as that of a sphere with mean interior density equal to 200 times the critical density of the Universe.
[3] We shall refer to the mid-point between the pair members as the 'barycentre' for short.

$V_r/\mathrm{km\,s^{-1}} < 0$, respectively, in order to approximate the present-day kinematics of the MW–M31 pair. Additionally, we impose a minimum mass ratio cut of $M_2/M_1 > 0.3\,(M_1 > M_2)$ to discard pairs with a large mass difference. Hereafter, we shall use 'DOVE pairs' to refer to all MedIso and HighIso pairs satisfying these conditions.

2.2 APOSTLE simulations

The APOSTLE project is a suite of cosmological hydrodynamical re-simulations of 12 volumes selected from the DOVE sample of LG candidate volumes discussed above (Sawala et al. 2016b; Fattahi et al. 2016). In addition to the kinematic constraints described in the DOVE selection, APOSTLE pair members satisfy a relative tangential velocity criterion, $V_t < 100\,\mathrm{km\,s^{-1}}$, and the surrounding haloes follow the Hubble flow out to ~ 4 Mpc, which is observed to be only weakly decelerated beyond ~ 1 Mpc (see Fattahi et al. 2016, for details). APOSTLE volumes are a subsample of the MedIso pairs described in the previous section, and are highlighted with circles in Fig. 1.

The APOSTLE simulations were run at three different levels of resolutions, labelled AP-L1, AP-L2, and AP-L3 with initial mass per gas particle of $\sim 10^4$, 10^5, and $10^6\,\mathrm{M_\odot}$, respectively, using the code developed for the EAGLE project (Schaye et al. 2015; Crain et al. 2015). All 12 APOSTLE volumes were simulated at resolution levels L2 and L3, but only five volumes have been simulated at resolution L1, due to the computational expense.

The EAGLE galaxy formation model was calibrated to reproduce the observed $z = 0.1$ stellar mass function of galaxies in the range $M_* \sim 10^8$–$10^{11}\,\mathrm{M_\odot}$, in a cosmological volume $(100^3\,\mathrm{Mpc^3})$, as well as the stellar mass–size relation of galaxies. The subgrid physics model includes metal cooling, star formation, stellar evolution and supernovae feedback, a homogeneous background UV/X-Ray photoionization radiation, supermassive black hole formation and evolution, and AGN feedback. The model reproduces the rotation curve of galaxies quite well (Schaller et al. 2015), as well as the Tully–Fisher relation over a wide range of masses (Ferrero et al. 2017; Sales et al. 2017).

Haloes, subhaloes, and galaxies in APOSTLE are also identified using the FoF and SUBFIND algorithms. Each APOSTLE volume has a dark matter-only (DMO) counterpart. We refer to the hydrodynamical and DMO runs as AP-HYDRO and AP-DMO, respectively.

3 GALAXY SAMPLES

3.1 Simulated galaxy sample

Galaxies and haloes in the simulated LG-like volumes are identified as bound structures, found by SUBFIND within 3 Mpc from the pair barycentre. We hereafter refer to the MW and M31 galaxy analogues as 'primaries'. Satellites are identified as galaxies (or subhaloes in the case of DMO runs) located within the virial radius of each of the primaries.

For the central system of each FoF halo, we define a galaxy stellar mass as that enclosed within a radius, $r_{gal} = 0.15 \times$ the virial radius of its halo. For subhaloes, where virial radii are ill defined, we use an average relation derived from the APOSTLE centrals: $r_{gal} = 0.169(V_{max}/\mathrm{km\,s^{-1}})^{1.01}$ kpc, where V_{max} is the maximum circular velocity of the system.[4]

3.2 The Local Group galaxy sample

Our main source of LG galaxies is the latest version of the LG catalogue of McConnachie (2012),[5] with a few updates with more recent discoveries (i.e. Crater II and Antlia II). We extend the catalogue with galaxies from the online Extragalactic Distance Database[6] (Tully et al. 2009) with reliable distance measurements, i.e. from the tip of the red giant branch or Cepheid variables methods.[7] This results in the addition of ~ 10 dwarf galaxies in the outskirts of the LG.

Our analysis uses the position, distance, V-band apparent magnitude, and half-light radius of a galaxy. We estimate stellar masses using the V-band stellar mass-to-light ratios given in table 1 of Woo, Courteau & Dekel (2008) for individual galaxies, or use their table 2 otherwise. Some field galaxies only have B-band magnitudes, in which case we use the B-band stellar mass-to-light ratios from Woo et al. (2008).

We define the LG volume as that of a 3 Mpc sphere centred at the mid-point between MW and M31.[8] Since r_{200} is not well known for either the MW and M31, we consider as 'satellites' any dwarf within 300 kpc from the centre of either MW or M31. We use the term 'Local Group field' galaxy to denote isolated galaxies (i.e. not MW or M31 satellites) within 3 Mpc from the LG barycentre.

4 THE DEMOGRAPHICS OF LG-LIKE ENVIRONMENTS

4.1 Total mass within 3 Mpc

We begin our analysis by considering the total mass of the LG-like volumes selected from DOVE. This is illustrated in Fig. 2, where we show, in the left-hand panel, $M_{3\mathrm{Mpc}}$, the total mass within 3 Mpc of each pair mid-point, versus the combined virial mass of the pair, $M_1 + M_2$. The vertical dashed line in Fig. 2 indicates the mass expected if the LG-like volumes had the same density as the average matter density of the universe. LG environments are clearly overdense, and the overdensity increases systematically with the combined mass of the pair.

All LG-like volumes lie below the 1:2 line in this plot, indicating that there is at least as much mass around the primaries as in the primaries themselves, and often much more. This is true even for the highly isolated pairs (HighIso, identified with crosses in Fig. 2), for which, on average, $M_{3\mathrm{Mpc}} \sim 3.7(M_1 + M_2)$. For APOSTLE volumes, which contain some MedIso and some HighIso volumes and are identified with red circles in Fig. 2, the average $M_{3\mathrm{Mpc}}/(M_1 + M_2)$ is 4.2.

We note that the extra mass outside the primary haloes is not expected to be distributed isotropically in the considered volume, but rather in filaments and sheet-like structures (see fig. 2 of Peñarrubia & Fattahi 2017, for a visual impression of mass distribution around APOSTLE volumes).

---

[4]The maximum circular velocity of a halo is a useful proxy of its virial mass. For isolated haloes, and at $z = 0$, the tight relation between the two may be approximated as $M_{200}/(10^{10}\,\mathrm{M_\odot}) = 19\,(V_{max}/100\,\mathrm{km\,s^{-1}})^{3.04}$, based on APOSTLE centrals.

[5]available from www.astro.uvic.ca/ alan/Nearby_Dwarf_Database.html.

[6]edd.ifa.hawaii.edu

[7]The majority of the distance measurements are based on Dalcanton et al. (2009), with the rest from Saha, Claver & Hoessel (2002), Karachentsev & Kashibadze (2006), Karachentsev et al. (2007), and Makarova et al. (2005).

[8]As for the simulated sample, we assume, for simplicity, that the 'LG barycentre' coincides with the mid-point between MW and M31.
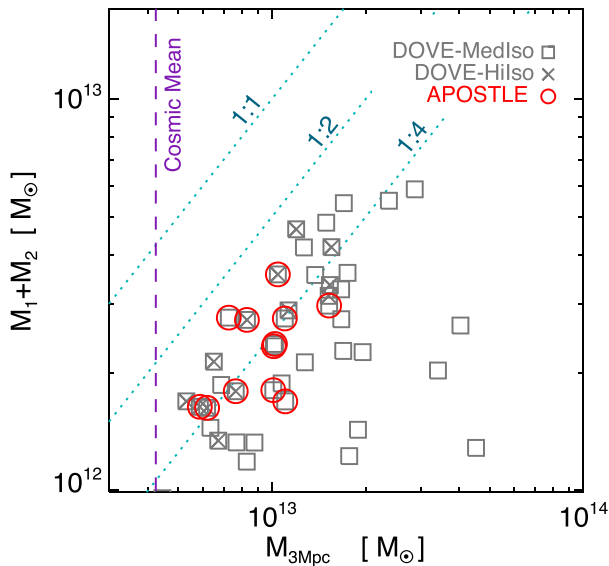
Figure 2. Combined virial mass of the pair, $M_1 + M_2$, versus the total mass, M_{3Mpc}, within a sphere of 3 Mpc radius centred on the barycentre, for MedIso and HiIso DOVE pairs. The vertical dashed line indicates M_{3Mpc} for a sphere with mean density equal to the mean matter density of the universe. The diagonal dotted lines show constant ratios between $M_1 + M_2$ and M_{3Mpc}, as indicated by their labels. APOSTLE candidates are marked with red circles.
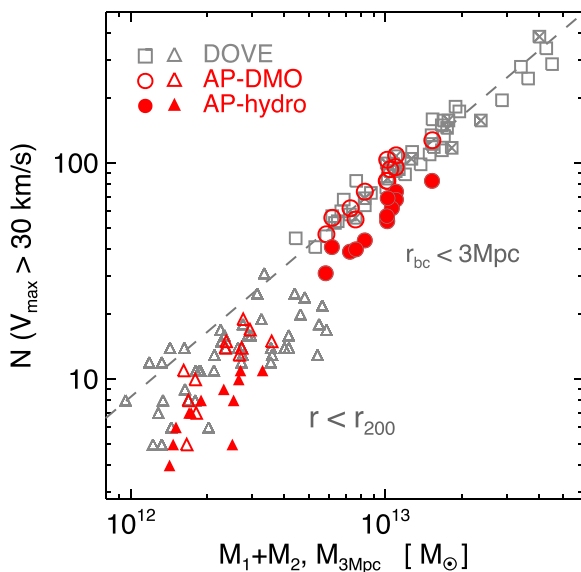

Figure 3. Total number of haloes/subhaloes with $V_{max} > 30 \, km \, s^{-1}$ within a 3Mpc-radius sphere centred on the pair barycentre, versus the total mass within the same volume, M_{3Mpc}, for MedIso (grey squares) and HiIso (crosses) DOVE pairs. Results for 12 APOSTLE DMO simulations and their hydrodynamical counterparts are shown as open and filled red circles, respectively. The triangles indicate subhaloes of the two primaries (satellites) versus the combined virial mass of the primaries.

4.2 Haloes and subhaloes

The higher the total LG mass, the larger the number of haloes (and, hence, galaxies) that it is expected to contain. We show this explicitly in Fig. 3, where the grey squares and circles indicate the *total* number of haloes and subhaloes in DMO runs with maximum circular velocity, V_{max}, exceeding 30 km s^{-1}. This velocity roughly corre-

sponds to the minimum mass expected of haloes that host dwarfs as luminous as the 'classical dSphs', i.e. those with $M_* > 10^5 \, M_\odot$ (e.g. Guo et al. 2010; Behroozi, Wechsler & Conroy 2013; Moster, Naab & White 2013; Sawala et al. 2015; Garrison-Kimmel et al. 2019).

The grey squares in Fig. 3 show the tight relation between the total number of such haloes and the total mass within 3 Mpc; indeed, the rms scatter around a 1:1 linear fit is only 0.1 dex. Filled red circles show the results for the AP-HYDRO runs, which also follow the 1:1 trend, but lie a factor of ~ 1.5 below the DMO results. This is because low-mass haloes (which dominate the total count) are affected by the loss of baryons driven by photoionization and supernova feedback. This loss stunts the mass growth of the haloes, leading to lower values of V_{max} than their DMO counterparts (Sawala, Scannapieco & White 2012; Sawala et al. 2016a).

Finally, the triangles in Fig. 3 indicate the number of subhaloes within the virial radii of the two primaries, as a function of their host virial mass ($M_1 + M_2$). Here, the effects of tidal stripping tend to depress systematically the numbers below extrapolations of the 1:1 trend seen at larger masses, as well as to increase the scatter. We have explicitly checked that the number of subhaloes does follow the same 1:1 trend as the primaries when using their peak maximum circular velocity, which is typically reached just before infall into the primary and is thus unaffected by tidal stripping.

4.3 Implications for the too-big-to-fail problem

The results from the previous section have implications for the 'too-big-to-fail (TBTF) problem in the field' raised by Garrison-Kimmel et al. (2014b, hereafter GK14). This problem concerns the number of haloes in DMO simulations that are too massive to be consistent with any observed galaxy with robust kinematic and photometric measurements. GK14 considered systems with $V_{peak} > 30 \, km \, s^{-1}$, where V_{peak} is the maximum value of V_{max} attained by a system throughout its history.

The counts of such objects in a volume defined by the combination of two spheres of radius 1.2 Mpc centred on each primary, but excluding their inner 300 kpc (which are populated by satellites), is reported to be in the range ~ 22–48 in the GK14 'ELVIS' simulations.[9] These were contrasted with the ~ 10 known galaxies with kinematic measurements consistent with $V_{peak} > 30 \, km \, s^{-1}$ haloes. The difference between the two is the basis for the TBTF problem in the field.

We revisit this issue in Fig. 4, where the open circles indicate the number of such haloes in the 12 AP-DMO simulations (L2), plotted as a function of the total mass, M_{out}, in the same 'hollowed-out spheres' used by GK14. As expected given our discussion in the previous subsection, the total number of haloes correlates strongly with M_{out}, which, in turn, correlates strongly with M_{3Mpc}. As in Fig. 3, the numbers are systematically reduced in the AP-HYDRO runs, due to the effect on V_{max} caused by the loss of baryons.

As the figure shows, half of all AP-HYDRO volumes have fewer than 22 systems with $V_{peak} > 30 \, km \, s^{-1}$ and two of them have 10 or fewer, reducing substantially the number of haloes without observed counterparts ('massive failures', in the parlance of GK14). The TBTF problem would only be manifest in volumes with total masses well in excess of $M_{3Mpc} \sim 10^{13} \, M_\odot$, which, as we shall discuss below, are disfavoured on other grounds.

This constraint on M_{3Mpc} implies that the total virial mass of primaries should be less than $M_1 + M_2 \sim 3 \times 10^{12} \, M_\odot$ (Fig. 2).

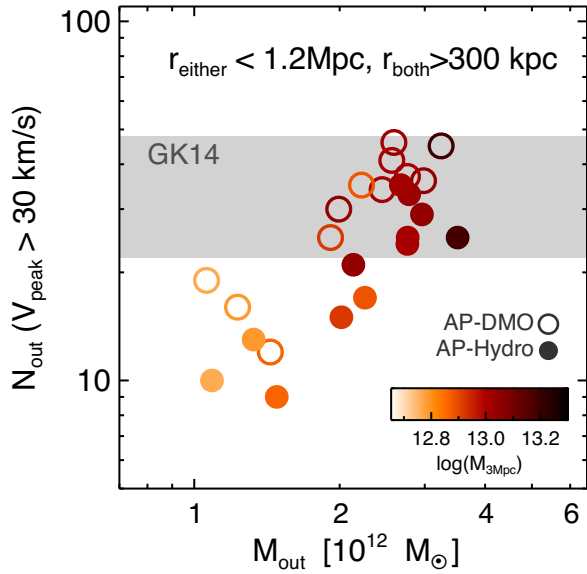[9] These values are estimated from fig. 6 of GK14 and can change by 1–2.

Figure 4. Number of haloes/subhaloes in AP-L2 simulations with V_{peak} exceeding 30 km s^{-1}, versus total mass, M_{out}, within the volume considered by GK14 in their study of the 'TBTF' problem in the LG field. The volume consists of two spheres, each of radius 1.2 Mpc, centred on the two primaries but excluding the inner 300 kpc of each. Note that, for the same volume, the total number of massive objects decreases by a factor of ∼1.5 from AP-DMO (DMO; open circles) to AP-HYDRO (filled circles), as noted by Sawala et al. (2013, 2015). The grey band spans the number of massive haloes in the ELVIS DMO simulations of Garrison-Kimmel et al. (2014a).

This is consistent with recent estimates of $M_1 + M_2$ based on the LG kinematics (Fattahi et al. 2016), and of the MW virial mass, $M_{200} \sim 10^{12}\,M_\odot$ (see e.g. Callingham et al. 2019, and references therein), if M31's virial mass does not exceed the Milky Way's by more than a factor of ∼2, as seems likely (Peñarrubia et al. 2016).

4.4 Galaxy formation efficiency

A similar trend with total LG mass to that described for haloes in Section 4.2 is seen for the number of simulated galaxies above a certain value of M_*. This is shown in Fig. 5, where we plot results for simulated galaxies with stellar mass exceeding 10^6, 10^7, and $5 \times 10^7\,M_\odot$. The linear trend is remarkably tight in all cases, and extends all the way to the satellites of individual primaries. This suggests that the tidal stripping effects that reduce the numbers of subhaloes above a fixed value of V_{max} (i.e. triangles in Fig. 3) are less important when considering stellar mass. This is not unexpected, as stars are confined to the bottom of the subhalo potential well, where they are harder to strip than the surrounding dark matter. Subhaloes can thus lose substantial amounts of dark matter before their stellar content is significantly altered.

The main lesson from Fig. 5 is that, at least in this mass range, the 'efficiency' of dwarf galaxy formation in or around the primaries of our LG simulations is remarkably similar. In other words, the number of dwarfs per unit mass is independent of whether the count is carried out over the virialized region of the primaries or over the whole LG volume. This implies that the fraction of all LG galaxies above a certain M_* that are satellites of either the MW or M31 should be approximately the same as the fraction of the total mass within 3 Mpc that is contained within the virial boundaries of the two primaries.

Note that this conclusion is insensitive to our adoption of the primary's virial radius to identify 'satellites'. Indeed, changing the definition from r_{200} to a fixed radius of 300 kpc, for example, would redefine primary masses and satellite numbers in similar proportion, simply shifting systems along the 1:1 line in Fig. 5. Although we do not show it here, we have explicitly checked that this is the case.

For example, there are 24 galaxies with $M_* > 5 \times 10^7\,M_\odot$ in the LG volume, 8 of which are satellites. The satellite fraction is thus ∼30 per cent, consistent with the ∼1:4 mass ratios inferred from Fig. 2. For $M_* > 10^7\,M_\odot$ the satellite fraction is also similar, with 12 satellites out of a total of 42 galaxies. These numbers seem to validate our simulation result that M_{3Mpc} should be roughly 3–4 times the combined virial mass of the primaries. Note that this
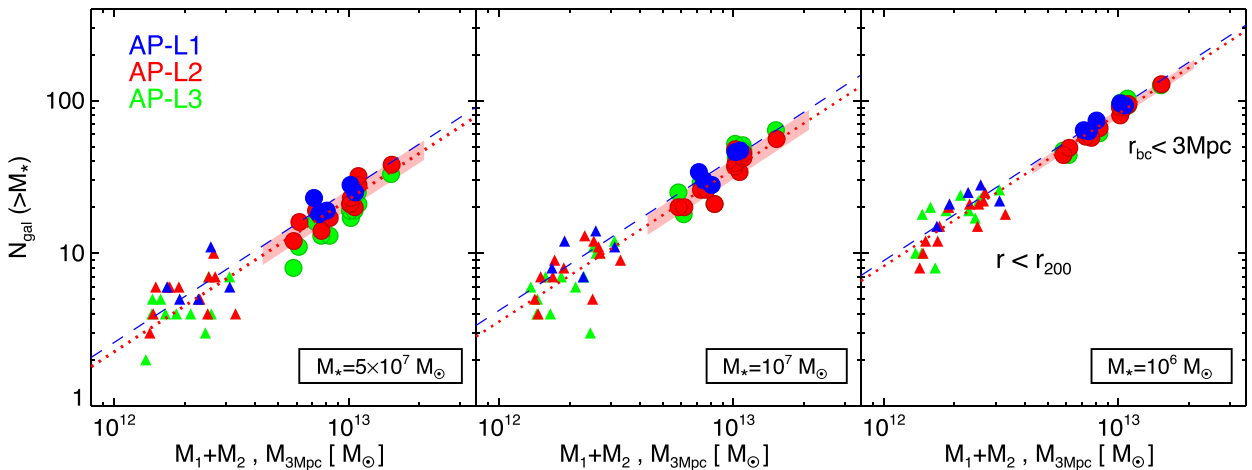

Figure 5. Number of galaxies above a given stellar mass, as specified in the legends, versus either M_{3Mpc} (circles) or the combined virial mass of the primaries, $M_1 + M_2$ (triangles) for AP-HYDRO simulations of varying resolution. Dotted and dashed lines are power-law fits with unity slope ($N \propto M$) to the AP-L1 and AP-L2 filled circles. The light red shaded regions represent the rms scatter around the AP-L2 fit. Note that the same fit equally well both circles and triangles, indicating that the dwarf galaxy formation efficiency in and around the primaries is very similar.
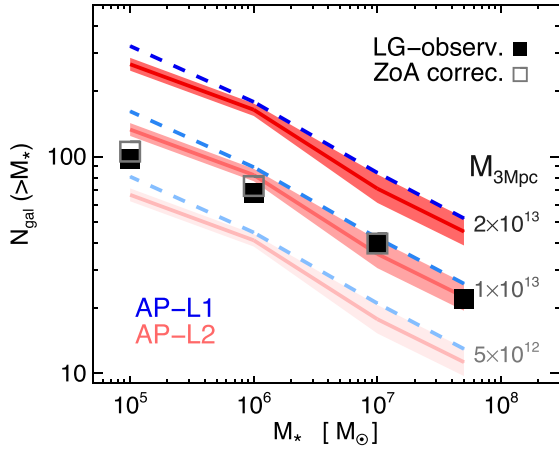
Figure 6. Predicted number of galaxies brighter than a given stellar mass from the fits to AP-HYDRO in Fig. 5, for different values of M_{3Mpc}. Blue (dashed) and red (solid) lines correspond to results for AP-L1 and AP-L2 fits, respectively. The observed number of galaxies in the LG is shown by the filled squares. Open squares are the same, corrected for galaxies possibly missing in the zone of avoidance (see text for details).
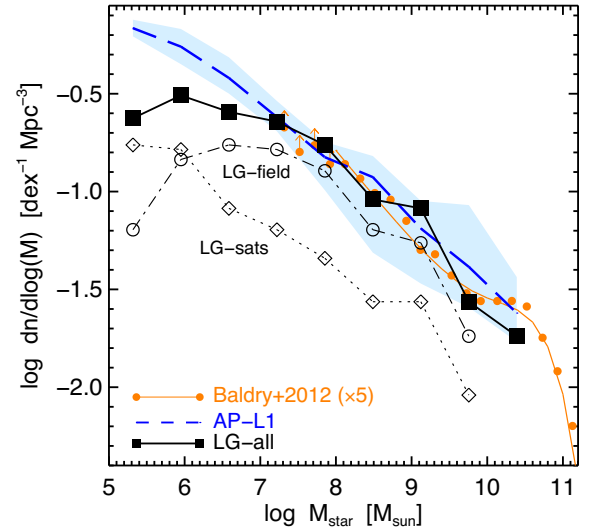

Figure 7. The observed stellar mass function of LG galaxies within 3 Mpc from the LG barycentre. Filled squares correspond to all known galaxies in that volume, while small circles and diamonds illustrate the contribution from field galaxies and from MW/M31 satellites. The average stellar mass function of five AP-L1 runs, each normalized to a common $M_{3Mpc} = 10^{13}\,M_\odot$ is shown by the solid blue line. The shaded blue region spans the full range of variation of individual runs. The field galaxy stellar mass function from Baldry et al. (2012) ($\times 5$), together with their double Schechter fit, are shown in orange.

conclusion is independent of the actual virial mass of the primaries, which are not accurately known (see Callingham et al. 2019, and references therein).

4.5 The total mass of the Local Group

The results of the previous subsection imply that, properly calibrated, the total number of dwarfs may be used as a proxy for the total mass, subject to an appropriate normalization. For example, the raw numbers of observed galaxies with $M_* > 5 \times 10^7$ or $> 10^7\,M_\odot$ may be used to infer the total mass of the LG, using the APOSTLE galaxy mass–halo mass relation, which is responsible for the vertical normalization of the lines in Fig. 5.

Coloured lines in Fig. 6 show the cumulative number of APOSTLE galaxies as a function of stellar mass for different values of M_{3Mpc}: 5×10^{12}, 10^{13}, and $2 \times 10^{13}\,M_\odot$, respectively. The line colours indicate AP-L2 (red) and AP-L1 (blue), and the shaded area is the 1σ scatter expected from the normalization uncertainty for AP-L2 runs. The observed numbers of galaxies (filled squares) with $M_* > 10^7\,M_\odot$ clearly favour $M_{3Mpc} \sim 10^{13}$, with a statistical uncertainty much smaller than a factor of 2. In particular, fitting AP-L2 results to galaxies with $M_* > 5 \times 10^7$ or $10^7\,M_\odot$ yield $M_{3Mpc} = (1.0 \pm 0.15) \times 10^{13}$ and $(1.18 \pm 0.17) \times 10^{13}\,M_\odot$ for each case, respectively. We emphasize that these estimates are sensitive to the APOSTLE normalization of the galaxy formation efficiency, which may vary for other models of star formation, feedback, and reionization.

We note that the estimated mass is sensitive to the minimum dwarf galaxy stellar mass chosen to match the curves in Fig. 6. Indeed, taken at face value, the total number of galaxies above $M_* = 10^5\,M_\odot$ would suggest almost a factor of two lower M_{3Mpc}. This implies that either the galaxy formation efficiency varies substantially with stellar mass in and around the LG primaries, or that our current LG inventory is missing about ~ 50 dwarfs at least as massive as $M_* = 10^5\,M_\odot$. We favour the latter explanation, not only because the former is at odds with the simulation results, but also because, as we discuss below, the evidence for incompleteness in the LG inventory below $10^7\,M_\odot$ is quite compelling.

4.6 Incompleteness in the LG inventory

We begin by noting that the incompleteness suggested by our discussion above is much larger than what may be expected purely from the highly extincted 'zone of avoidance' delineated by the Galactic disc. This area obscures a region of roughly ± 15 deg around the Galactic plane, which translates into ~ 30 per cent of the available sky. Correcting for this effect[10] would only lift the number of $M_* > 10^5\,M_\odot$ field dwarfs by ~ 8, as shown by the open symbols in Fig. 6. This is much smaller than is required to bring the number of $M_* > 10^5\,M_\odot$ dwarfs into agreement with what is expected for $M_{3Mpc} = 10^{13}\,M_\odot$.

Compelling evidence for incompleteness comes from the observed LG galaxy stellar mass function, shown by the filled squares in Fig. 7. For $M_* > 10^7\,M_\odot$, the shape of this function compares well with that of Baldry et al. (2012, suitably scaled),[11] as well as with the AP-L1 galaxy mass function (blue curve and shaded region), normalized to $M_{3Mpc} = 10^{13}\,M_\odot$. Below $10^7\,M_\odot$, however, the observed LG mass function flattens and becomes much shallower than for APOSTLE . This flattening of the mass function below $10^7\,M_\odot$ is a sign of incompleteness and is the reason behind the deficit of dwarf galaxies at $10^5\,M_\odot$ highlighted when discussing Fig. 6.

The open circles (corresponding to observed LG field galaxies) and diamonds (satellites) show that the flattening is entirely driven

---

[10]The correction is estimated by assuming the number density of galaxies inside the zone of avoidance is similar to the number density outside it.

[11]The scaling shown in Fig. 7 is different from the one expected from the M_{3Mpc} estimates of Section 4.5. This is because the APOSTLE galaxy stellar mass function, like that of the EAGLE simulation, does not match perfectly the Baldry et al. (2012) results. We refer the reader to Schaye et al. (2015) for further details on this issue.

by a pronounced lack of low-mass galaxies in the field: the MW and M31 satellites have a steeper faint-end slope, actually consistent in shape with that of the APOSTLE mass function. This is in agreement with Newton et al. (e.g. 2018), who have argued that the luminosity function of MW satellites is almost complete above $M_* \gtrsim 10^5\,\mathrm{M_\odot}$ (i.e. $M_V \lesssim -8$).

The flattening in the LG stellar mass function below $10^7\,\mathrm{M_\odot}$ is thus most likely the result of incompleteness in existing catalogues, as satellites are easier to find than LG field dwarfs. Indeed, they are closer to the Sun in the case of the Milky Way, and they are concentrated in a smaller region of the sky in the case of M31, which makes them easier to survey to faint levels (e.g. Pan-Andromeda Archaeological Survey, PAndAS, Martin et al. 2006; McConnachie et al. 2009).

4.7 Missing dwarfs in the Local Group

The discussion above implies that ~ 50 dwarf galaxies with stellar mass greater than $10^5\,\mathrm{M_\odot}$ are missing from the current LG inventory. This prediction depends solely on assuming that the efficiency of dwarf galaxy formation is uniform throughout the volume (as found in the simulations) and that the inventory of the most luminous dwarfs is complete. Or, in other words, these are the number of missing dwarfs in the field required to make the satellite fraction of $M_* > 10^5\,\mathrm{M_\odot}$ dwarfs the same as that of galaxies with $M_* > 10^7\,\mathrm{M_\odot}$.

Where are these missing galaxies located? Naively, one might anticipate that they are predominantly near the outer edge of the 3 Mpc sphere, where much of the volume resides. The simulations, however, suggest otherwise. We show this in Fig. 8, where the blue curve in the top panel shows the average cumulative radial distribution of galaxies more massive than $10^6\,\mathrm{M_\odot}$ (plus scatter) in AP-L1 volumes, measured from their barycentre, after normalizing them to a common mass of $M_{\mathrm{3Mpc}} = 1 \times 10^{13}\,\mathrm{M_\odot}$; the bottom panel shows the results for simulated galaxies more massive than $10^5\,\mathrm{M_\odot}$.

According to the APOSTLE results, nearly half of all galaxies are expected to be within the inner 1 Mpc (i.e. in the inner ~ 4 per cent of the full volume), and 75 per cent are expected to be within 2 Mpc, occupying only the inner ~ 30 per cent of the volume. As anticipated by our earlier discussion on galaxy formation efficiency, Fig. 9 shows that the cumulative radial distribution of galaxies neatly tracks the distribution of mass within the APOSTLE volumes.

Indeed, most of the 'missing dwarfs' are expected to be within 1.5 Mpc of the LG barycentre, mainly clustered in the outskirts of the haloes of the two primaries. This is illustrated in Fig. 10, which shows, in an Aitoff all-sky projection and viewed from the MW perspective, the location of all AP-L1 field galaxies with $M_* > 10^5\,\mathrm{M_\odot}$ (all five AP-L1 volumes combined; see small blue circles). The coordinate system is defined so that the M31 analogues are located in the same sky position as in observations. Observed field dwarfs are presented as black circles, and MW and M31 satellites as green and red ones, respectively. Interestingly, APOSTLE predicts that (missing) field dwarf galaxies are *not* randomly located on the sky, but more likely towards M31's direction,[12] with some of them being closer than 1 Mpc to the MW (open circles).

---

[12]This is consistent with observations; McConnachie (2012) points out that known field dwarf galaxies in the LG are located preferentially towards M31 in the sky.
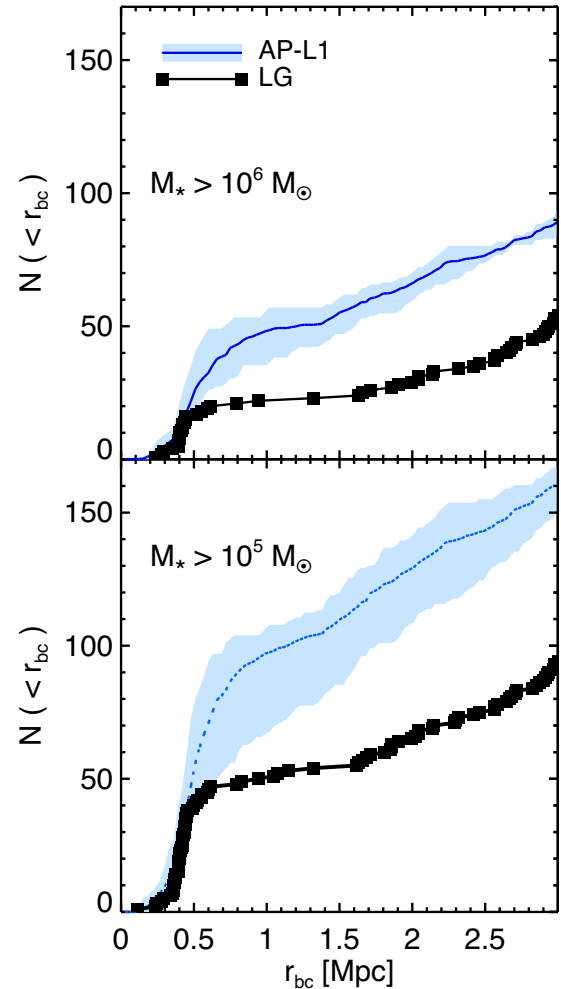

Figure 8. *Top*: The cumulative radial distribution of observed LG galaxies with stellar mass above $10^5\,\mathrm{M_\odot}$, shown as connected filled squares. Radii are measured from the LG barycentre. The solid blue line indicates the results expected from AP-L1 runs, normalized to a common mass of $M_{\mathrm{3Mpc}} = 10^{13}\,\mathrm{M_\odot}$. The shaded region illustrates the full range of variations for individual AP-L1 runs. *Bottom*: Same as top panel but for the stellar mass cut of $M_{\mathrm{str}} > 10^6\,\mathrm{M_\odot}$.

Why have these dwarfs been missed? The most likely explanation is that they are extended, LSB systems that do not stand out in panoramic surveys. This is easily appreciated in Fig. 11, where we show the *V*-band luminosity and stellar half-mass radius of all LG dwarfs, if available. MW and M31 satellites are shown by open circles, whereas LG field dwarfs are indicated by filled squares. Dashed lines indicate constant effective surface brightness, each separated by one dex, and starting, at the top, at $10^6\,\mathrm{L_\odot\,kpc^{-2}}$ (i.e. $\sim 26.5\,m_V\,\mathrm{arcsec^{-2}}$).

Note that this is already below the effective surface brightness of UDGs such as the Coma cluster Dragonfly galaxies (DF, shown for reference with starred green symbols, van Dokkum et al. 2015). Clearly, many observed LG galaxies are extremely LSB systems far fainter than typical UDGs. Such LG galaxies are typically resolved into individual stars and their discovery relies on special methods based on searching for overdensities after filtering stars with isochrone masks (see e.g. Koposov et al. 2008).

The extreme LSB regime probed by LG dwarfs reaches, in the case of And XIX or Crater II, approximately $\Sigma_{\mathrm{eff}} \sim 30\,m_V\,\mathrm{arcsec^{-2}}$.
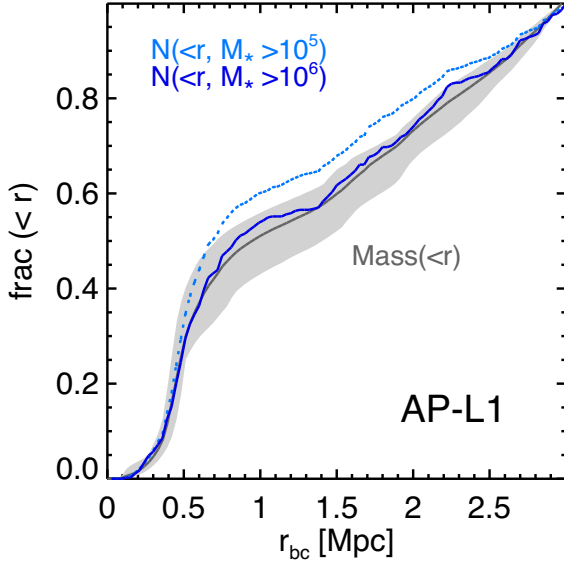
Figure 9. Average cumulative mass profile of AP-L1 runs, normalized to their $M_{3\mathrm{Mpc}}$ (in grey). Curves indicate cumulative numbers of galaxies with $M_* > 10^5\,\mathrm{M_\odot}$ (cyan) or $M_* > 10^6\,\mathrm{M_\odot}$ (blue), respectively. Note that the number of galaxies traces closely the mass distribution in the LG simulations.

Indeed, $\sim$40 per cent of all known LG satellites with $M_* > 10^5\,\mathrm{M_\odot}$ have effective surface brightness below the Coma UDGs. By contrast, only *one* LG field galaxy, Eri II, has an effective surface brightness below $10^6\,\mathrm{L_\odot\,kpc^{-2}}$. Eri II was discovered relatively recently and is located just outside 300 kpc from the MW (Li et al. 2017).

Fig. 11 also suggests that, in the range $10^5 < M_*/\mathrm{M_\odot} < 10^6$, the properties of the missing galaxies should be similar to those of M31 satellites such as And XIV, And XIX, or And XXIII, which were identified in the PAndAS survey at a distance of $\sim$700 kpc (we emphasize that these are *not* 'ultrafaint' dwarfs, but, rather, systems with luminosities comparable to that of 'classical' dSphs). Putting all these results together, we conclude that a PAndAS-like survey of the outskirts of the M31–M33 system, if deep enough to detect systems like the aforementioned M31 satellites out to 1.5–2 Mpc, should be able to net the majority of the isolated dwarfs missing from our current inventory of the LG. We note that at a distance of 1.5 Mpc, even stars as bright as blue horizontal branch stars would have magnitudes $m_V \sim 26$.

5 SUMMARY

We have analysed the environment of galaxy pairs with mass and kinematics resembling the Milky Way and Andromeda galaxies in
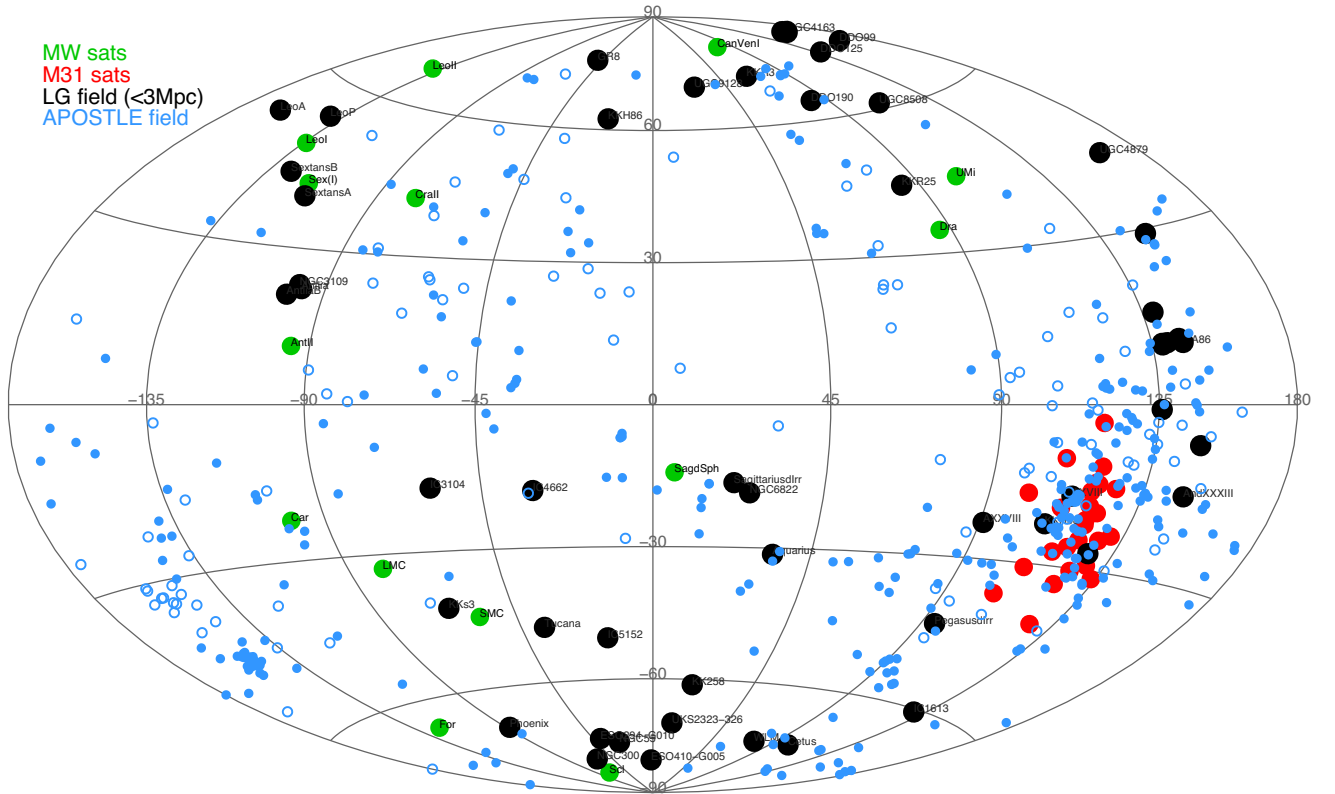
Figure 10. Aitoff projection of observed LG dwarf galaxies with stellar mass above $10^5\,\mathrm{M_\odot}$, in Galactic coordinates. MW and M31 satellites are shown with green and red symbols, respectively. LG field dwarfs (i.e. within 3 Mpc from the LG barycentre) are shown with large black circles. Simulated *field* dwarf galaxies with $M_* > 10^5\,\mathrm{M_\odot}$ in five AP-L1 simulations are shown with small blue circles. Open and field symbols indicate whether the simulated dwarf is closer or farther than 1 Mpc from the MW analogue, respectively. The simulation coordinates are centred on the MW analogues and rotated so that the M31 analogues are in the same sky location as M31; i.e. $(l, b) = (121.2°, -21.6°)$. Note that many missing dwarfs are expected to be in the region that immediately surrounds M31, but most are expected to be more than 1 Mpc away, and thus may have been missed by existing surveys.
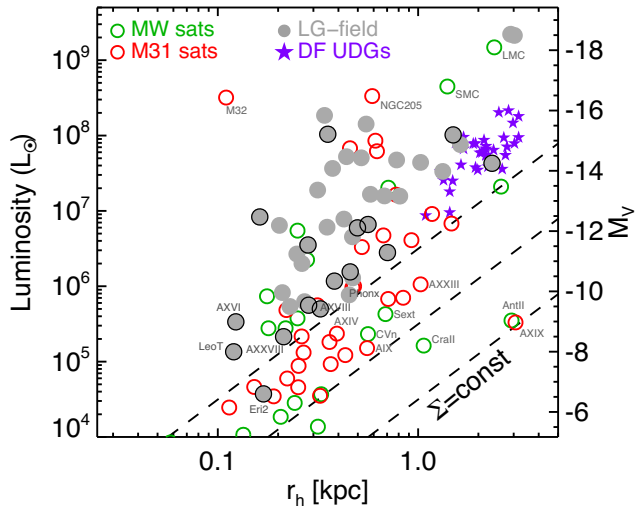
Figure 11. Luminosity versus half-light radii of observed LG field and satellite dwarf galaxies, shown as filled squares and open circles, respectively. Field galaxies with σ_{los} measurements are highlighted with black squares. For comparison, Dragonfly UDGs of the Coma cluster (van Dokkum et al. 2015) are shown as green starred symbols. We use r-band luminosities for these galaxies. The diagonal lines illustrate lines of constant effective surface brightness, each separated by 1 dex and corresponding to $\Sigma_{eff} = 10^6$, 10^5, and $10^4\, L_\odot\, kpc^{-2}$, equivalent to roughly 26.5, 29, and 31.5 $m_V\, arcsec^{-2}$.

the DOVE N-body simulation of a large cosmological volume. We find that the total mass within 3 Mpc from the pair mid-point (which we define as the LG boundary) is typically ~ 4 times the combined virial mass of the pair. In general, within that volume there is always at least as much mass within the virial boundaries of the primaries as in their surroundings.

Cosmological hydrodynamical re-simulations of many of those pairs (from the APOSTLE Project) show that the dwarf galaxy formation efficiency, defined as the total number of dwarfs above a certain stellar mass per unit mass, is uniform throughout the volume and thus similar in and around the primaries. This implies that the total number of dwarfs within 3 Mpc, or within the virial volume of each primary, depends solely on the total mass of that volume.

These two results indicate that satellites should make up about 1/4 of all dwarf galaxies in the LG. Although this prediction is approximately correct for observed dwarfs more massive than $M_* = 10^7\, M_\odot$, the agreement becomes gradually worse for less massive galaxies: satellites make up more than 40 per cent of those with $M_* > 10^5\, M_\odot$. We interpret this as a result of incompleteness in existing LG dwarf galaxy catalogues, and predict that there are ~ 50 dwarfs at least as massive as the Draco dSph (i.e. $M_* \sim 10^5\, M_\odot$) missing from our current LG inventory.

Our interpretation is supported by (i) the faint-end shape of the LG field galaxy luminosity function, which, unlike that of satellites, becomes abruptly shallow below $M_* \sim 10^7\, M_\odot$, and by (ii) the lack of LG field galaxies with effective surface brightness below $\sim 10^6\, L_\odot\, kpc^{-2}$.

The simulations indicate that the missing dwarfs should cluster tightly around the two primaries. Indeed, most of them should be within 1.5 Mpc from the LG barycentre. Additionally, a notable fraction is expected to lie around M31 in the sky. These are strong predictions that might be possible to verify with upcoming wide-field deep imaging surveys, such as that planned by the

Large Synoptic Survey Telescope or the Canada–France Imaging Survey, if existing methods for detecting dwarfs using ground-based imaging can be improved enough to target such objects, or if planned wide-field imaging surveys from space (such as that envisioned by the MESSIER and CASTOR[13] missions; Valls-Gaubaud & MESSIER collaboration 2017, Côte et al. 2012) come to fruition.

If proven correct, our results have strong implications for a number of current discussions regarding perceived failures of the ΛCDM paradigm in the LG. Issues such as the 'TBTF' problem in the field (GK14), where the kinematics of observed dwarfs are used to infer their halo masses, whose abundance is, in turn, compared with simulations, can be singularly affected. In particular, if the total mass of the LG is about $M_{3Mpc} \sim 10^{13}\, M_\odot$, the total number of massive haloes without observed counterparts is not significant, especially when considering the reduction in mass that low-mass haloes experience because of the loss of baryons as a result of reionization and feedback (Sawala et al. 2013, 2015).

Finally, the fraction of known dwarfs in the LG volume with kinematic measurements is relatively small (only ~ 30 per cent of LG field dwarfs have published velocity dispersion), and our results raise the possibility that many existing dwarfs may actually be missing from current catalogues. As the LG inventory of dwarf galaxies becomes increasingly complete, it is likely that our understanding of dwarf galaxy formation in our immediate cosmic neighbourhood, and its cosmological significance, will become clearer.

REFERENCES

Baldry I. K. et al., 2012, MNRAS, 421, 621
Beasley M. A., Romanowsky A. J., Pota V., Navarro I. M., Martinez Delgado D., Neyer F., Deich A. L., 2016, ApJ, 819, L20
Bechtol K. et al., 2015, ApJ, 807, 50
Behroozi P. S., Wechsler R. H., Conroy C., 2013, ApJ, 770, 57
Belokurov V. et al., 2007, ApJ, 654, 897

[13]http://orca.phys.uvic.ca/ pcote/castor/

Belokurov V. et al., 2010, ApJ, 712, L103

Caldwell N. et al., 2017, ApJ, 839, 20

Callingham T. M. et al., 2019, MNRAS, 484, 5453

Collins M. L. M. et al., 2013, ApJ, 768, 172

Côte P. et al., 2012, in Clampin M. C., Fazio G. G., MacEwen H. A., Oschmann J. M. Jr, eds, Proc. SPIE Conf. Ser. Vol. 8442, Space Telescopes and Instrumentation 2012: Optical, Infrared, and Millimeter Wave. SPIE, Bellingham, p. 844215

Crain R. A. et al., 2015, MNRAS, 450, 1937

Dalcanton J. J. et al., 2009, ApJS, 183, 67

Davis M., Efstathiou G., Frenk C. S., White S. D. M., 1985, ApJ, 292, 371

Drlica-Wagner A. et al., 2015, ApJ, 813, 109

Fattahi A. et al., 2016, MNRAS, 457, 844

Ferrero I. et al., 2017, MNRAS, 464, 4736

Garrison-Kimmel S., Boylan-Kolchin M., Bullock J. S., Lee K., 2014a, MNRAS, 438, 2578

Garrison-Kimmel S., Boylan-Kolchin M., Bullock J. S., Kirby E. N., 2014b, MNRAS, 444, 222 (GK14)

Garrison-Kimmel S. et al., 2019, MNRAS, 487, 1380

Gregory A. L., Collins M. L. M., Read J. I., Irwin M. J., Ibata R. A., Martin N. F., McConnachie A. W., Weisz D. R., 2019, MNRAS, 485, 2010

Guo Q., White S., Li C., Boylan-Kolchin M., 2010, MNRAS, 404, 1111

Jenkins A., 2013, MNRAS, 434, 2094

Kahn F. D., Woltjer L., 1959, ApJ, 130, 705

Karachentsev I. D., Kashibadze O. G., 2006, Astrophysics, 49, 3

Karachentsev I. D. et al., 2007, AJ, 133, 504

Komatsu E. et al., 2011, ApJS, 192, 18

Koposov S. et al., 2008, ApJ, 686, 279

Koposov S. E. et al., 2011, ApJ, 736, 146

Koposov S. E., Belokurov V., Torrealba G., Evans N. W., 2015, ApJ, 805, 130

Li Y.-S., White S. D. M., 2008, MNRAS, 384, 1459

Li T. S. et al., 2017, ApJ, 838, 8

Makarova L. N., Karachentsev I. D., Grebel E. K., Harbeck D., Korotkova G. G., Geisler D., 2005, A&A, 433, 751

Martin N. F., Ibata R. A., Irwin M. J., Chapman S., Lewis G. F., Ferguson A. M. N., Tanvir N., McConnachie A. W., 2006, MNRAS, 371, 1983

Martin N. F. et al., 2016, MNRAS, 458, L59

McConnachie A. W., 2012, AJ, 144, 4

McConnachie A. W. et al., 2008, ApJ, 688, 1009

McConnachie A. W. et al., 2009, Nature, 461, 66

Moster B. P., Naab T., White S. D. M., 2013, MNRAS, 428, 3121

Nadler E. O., Mao Y.-Y., Green G. M., Wechsler R. H., 2019, ApJ, 873, 34

Newton O., Cautun M., Jenkins A., Frenk C. S., Helly J. C., 2018, MNRAS, 479, 2853

Peñarrubia J., Fattahi A., 2017, MNRAS, 468, 1300

Peñarrubia J., Gómez F. A., Besla G., Erkal D., Ma Y.-Z., 2016, MNRAS, 456, L54

Saha A., Claver J., Hoessel J. G., 2002, AJ, 124, 839

Sales L. V. et al., 2017, MNRAS, 464, 2419

Sawala T., Scannapieco C., White S., 2012, MNRAS, 420, 1714

Sawala T., Frenk C. S., Crain R. A., Jenkins A., Schaye J., Theuns T., Zavala J., 2013, MNRAS, 431, 1366

Sawala T. et al., 2015, MNRAS, 448, 2941

Sawala T. et al., 2016a, MNRAS, 456, 85

Sawala T. et al., 2016b, MNRAS, 457, 1931

Schaller M. et al., 2015, MNRAS, 451, 1247

Schaye J. et al., 2015, MNRAS, 446, 521

Simon J. D., 2019, ARA&A, 57, 375

Simon J. D., Geha M., 2007, ApJ, 670, 313

Springel V., Yoshida N., White S. D. M., 2001, New Astron., 6, 79

Springel V. et al., 2005, Nature, 435, 629

Tolstoy E., Hill V., Tosi M., 2009, ARA&A, 47, 371

Torrealba G., Koposov S. E., Belokurov V., Irwin M., 2016, MNRAS, 459, 2370

Torrealba G. et al., 2018, MNRAS, 475, 5085

Tully R. B., Rizzi L., Shaya E. J., Courtois H. M., Makarov D. I., Jacobs B. A., 2009, AJ, 138, 323

van Dokkum P. G., Abraham R., Merritt A., Zhang J., Geha M., Conroy C., 2015, ApJ, 798, L45

van Dokkum P. et al., 2016, ApJ, 828, L6

van Dokkum P. et al., 2018, Nature, 555, 629

Walker M. G., Mateo M., Olszewski E. W., Gnedin O. Y., Wang X., Sen B., Woodroofe M., 2007, ApJ, 667, L53

Walker M. G. et al., 2016, ApJ, 819, 53

Woo J., Courteau S., Dekel A., 2008, MNRAS, 390, 1453

Yagi M., Koda J., Komiyama Y., Yamanoi H., 2016, ApJS, 225, 11

Valls-Gabaud D., Messier Collaboration, 2017, in Gil de Paz A., Knapen J. H., Lee J. C., eds, IAU Symposium Vol. 321, Formation and Evolution of Galaxy Outskirts, p. 99

This paper has been typeset from a TEX/LATEX file prepared by the author.